Mitochondrial Creatine Kinase Binding to Phospholipid Monolayers Induces Cardiolipin Segregation

Ofelia Maniti,[†‡] Marie-France Lecompte,[§] Olivier Marcillat,[†] Bernard Desbat,[¶] René Buchet,[†‡] Christian Vial,[†‡] and Thierry Granjon[†‡*]

[†]Chemistry-Biochemistry, Université de Lyon, Lyon, France; [‡]Unite Mixte de Recherche 5246, Centre National de la Recherche Scientifique, l'Institut Multidisciplinaire de Biochimie des Lipides, Institut de Chimie et Biochimie Moléculaires et Supramoléculaires, Université Lyon 1, Villeurbanne, France; [§]Faculté de Médecine de Rangueil, Université Paul Sabatier, Toulouse, France; and [¶]Unite Mixte de Recherche 5248, Centre de Biophysique Moléculaire Numérique, Centre National de la Recherche Scientifique, École Nationale d'Ingénieurs des Travaux Agricoles de Bordeaux, Université Bordeaux 1, Pessac, France

ABSTRACT It is well established that the octameric mitochondrial form of creatine kinase (mtCK) binds to the outer face of the inner mitochondrial membrane mainly via electrostatic interactions with cardiolipin (CL). However, little is known about the consequences of these interactions on membrane and protein levels. Brewster angle microscopy investigations provide, for the first time to our knowledge, images indicating that mtCK binding induced cluster formation on CL monolayers. The thickness of the clusters (10–12 nm) corresponds to the theoretical height of the mtCK-CL complex. Protein insertion into a condensed CL film, together with monolayer stabilization after protein addition, was observed by means of differential capacity measurements. Polarization modulation infrared reflection-absorption spectroscopy showed that the mean orientation of α-helices within the protein shifted upon CL binding from 30° to 45° with respect to the interface plane, demonstrating protein domain movements. A comparison of data obtained with CL and phosphatidylcholine/phosphatidylethanolamine/CL (2:1:1) monolayers indicates that mtCK is able to selectively recruit CL molecules within the mixed monolayer, consolidating and changing the morphology of the interfacial film. Therefore, CL-rich domains induced by mtCK binding could modulate mitochondrial inner membrane morphology into a raft-like organization and influence essential steps of mitochondria-mediated apoptosis.

INTRODUCTION

The interaction between the mitochondrial octameric isoform of creatine kinase (mtCK)[2] and the outer side of the inner mitochondrial membrane is an important structural factor that may modulate the distribution of energy in cells of excitable tissues (1). Moreover, by stabilizing contact sites between the outer and inner mitochondrial membranes (2), mtCK may be involved in regulating the permeability transition pore (3–5). Experiments performed with mitochondria from transgenic mice expressing mtCK in liver cells, which are normally devoid of this enzyme, showed that mtCK plays a role in mitochondrial morphology (6,7). Results obtained by silencing mtCK RNA in HaCaT and HeLaS3 cell lines corroborate these findings, as the mitochondrial morphology was severely altered (8). Membrane binding occurs mainly via electrostatic interactions between cardiolipin (CL) (9) and the positively charged residues of the protein C-terminal end (Lys^{380}, Lys^{379}, and Lys^{369}) (10); however, hydrophobic interactions may also be involved (10). The mitochondrial isoforms exist as two interconvertible oligomeric states: a dimer and an octamer. Only the octamer binds to natural or biomimetic membranes (11–13). MtCK binding to CL-containing liposomes decreases the fluidity of the membrane and induces only small structural changes in the protein, namely, a slight modification of the β-sheet/α-helix ratio (14). These modifications are abolished by the addition of enzyme adenylic substrates, indicating that the protein is desorbed from the liposomes (15). The effects of this phenomenon on mtCK activity and its physiological role have not yet been clarified.

CL is present exclusively in mitochondrial membranes (25% of the inner membrane (16) and 4% of the outer membrane (17)) and is required for optimal activity of electron transport chain complexes involved in oxidative phosphorylation (18–20) or of adenine nucleotide translocator (ANT) (21). Therefore, any modification of CL distribution in the membrane can affect energetic metabolism. Accumulating evidence suggests that this unique lipid is also involved in several of the mitochondria-dependent steps of apoptosis (22). These steps include interactions of the Bcl-2 family of proteins, cytochrome *c* association and dissociation, and structure alteration of mitochondrial inner membrane. By analogy with sphingomyelin, a plasma-membrane lipid present in rafts and involved in recognition and signaling on the cell surface (23), it has been suggested that CL is involved in the formation of signaling platforms in mitochondrial membranes (22). CL domains in bacterial membranes have been observed in *Escherichia coli* (24) and in the polar septal membrane of *Bacillus subtilis* during sporulation (25). Because CL is essential for association of complexes III and IV into a supercomplex, it was suggested that redox complexes in mitochondria and bacteria may be assembled in CL-enriched domains (26,27), and that ANT and mtCK are functionally coupled (1,28,29); however, no direct interaction was observed. Since both proteins show

Submitted July 22, 2008, and accepted for publication December 15, 2008.

*Correspondence: thierry.granjon@univ-lyon1.fr

Editor: Paul H. Axelsen.

0006-3495/09/03/2428/11 $2.00

doi: 10.1016/j.bpj.2008.12.3911

a high affinity for CL, they may interact through CL patches (30). CL segregation induced by mitochondrial proteins in model membranes containing CL and either dipalmitoylphosphatidylethanolamine or 1-palmitoyl-2-oleoylphosphatidylethanolamine was suggested by differential scanning calorimetry results (31).

In this report, we describe the organization of CL-rich domains induced by mtCK binding to phospholipid monolayers at the air-buffer interface, as directly visualized by Brewster angle microscopy (BAM). Further information on the protein-lipid interaction was obtained by polarization modulation infrared reflexion spectroscopy (PM-IRRAS) and alternative current (a.c.) polarography. Protein-domain movements were observed upon membrane binding together with protein insertion into a condensed monolayer. Such CL-rich domains formed upon reversible binding of mtCK to the inner mitochondrial membrane are of structural and functional importance because they can alter the activity of membrane proteins, such as electron transport chain complexes or ANT, or modulate membrane binding of molecules involved in the apoptosis process, particularly cytochrome *c* and Bcl-2 family proteins.

MATERIALS AND METHODS

Materials

Tris, dithiothreitol (DTT), NaCl, egg yolk phosphatidylcholine (PC), egg yolk phosphatidylethanolamine (PE), and bovine heart CL were obtained from Sigma (Saint Quentin Fallavier, France). They were of the highest purity available. Ultrapure water was obtained from a Millipore system. For a.c. polarography measurements, chromatographically homogeneous egg yolk PC and PE in chloroform-methanol solution were purchased from Lipid Products (Nutfield, United Kingdom). Mercury was purified and doubly distilled under vacuum.

Protein expression and purification

Recombinant octameric rabbit heart mtCK (340 kDa) was purified as described elsewhere (32). The purified enzyme was obtained in 20 mM Tris-HCl, 0.1 mM EDTA, and 0.2 mM DTT pH 7.4 buffer, at a protein concentration of 0.2 g/L. Protein concentration was determined by the Lowry method using bovine serum albumin as the standard.

Film formation and surface pressure measurements for BAM and PM-IRRAS

A circular Teflon trough (Riegler & Kirstein, Postdam, Germany) was filled with 30 mL 20 mM Tris-HCl buffer, pH 7.4. Phospholipid monolayers were formed on a clean air-buffer interface by spreading the phospholipids dissolved in chloroform/methanol (4:1) to attain a lateral surface pressure of ~30 mN/m. After pressure stabilization, a final concentration of 4 nM mtCK was injected in the subphase. In the case of PM-IRRAS spectra recorded in the presence of a PC/PE/CL (2:1:1) mixture, 8 nM mtCK was injected in the subphase to increase the quality of the signal. Measurements were taken at 20°C.

BAM measurements

A commercial Brewster angle microscope manufactured by NFT (Göttingen, Germany) mounted on a trough was used to determine the morphology of the phospholipid film (33,34) in the presence or absence of protein. The microscope was equipped with a 532 nm laser, a polarizer, an analyzer, and a CCD camera. The BAM image size was 430 × 540 μm with 2 μm spatial resolution. The measurements were performed at different shutter speeds (integration time) ranging from 1:250 to 1:2000 s to adapt to different illumination levels. Camera calibration was necessary to determine the relationship among the measured intensity parameter for different shutter speeds, the gray level (GL), and the reflectance (*I*). This was done following a previously described procedure (35,36). Thus, we could calculate the reflectance as follows:

$$I = (\mathrm{GL} - \mathrm{B}G) \times F,$$

where GL is the recorded gray level value, BG is the background value of the camera, and F is the calibration factor for each shutter speed. For ultrathin films, the reflectance depends on both the thickness and refractive index of the monolayer:

$$I \propto \lambda d^2 n^2,$$

where λ is the laser wavelength, d is the film thickness, and n is the refractive index of the interfacial film. For a measured reflectance and at a given refractive index, the BAM software allows modeling of the average or local thickness of the film. A refractive index of 1.46, which corresponds to a monolayer in a rather fluid state (37–40), was used for the lipid monolayer. The refractive index of proteins generally varies in a relatively small range, between 1.36 and 1.55, depending on the size of the molecule and the type of the interface (41). Considering the size of mtCK, a refractive index of 1.4–1.45 should be expected. Because the density of lipids at the interface was relatively high, for a mixed mtCK-lipid monolayer the refractive index was considered to be close to that of the pure lipid: 1.46. The different views of the interfacial film were reconstituted using the BAM software 3D viewer (NFT, Göttingen, Germany) based on the brightness of the BAM pictures.

Alternative current polarographic measurements

For electrochemical measurements, PC, CL, and PC/PE/CL (2:1:1) mixture dried samples were dissolved in hexane. Measurements of the differential capacity (C) of a hanging mercury drop electrode with respect to the potential (C versus E) were carried out as described elsewhere in a Metrohm polarographic cell (42). Phospholipids were added until a stable and constant value of C in a wide potential range between −0.2 and −0.7 V was reached. In our experiments, 0.6 μg/cm^2 PC, 0.2 μg/cm^2 CL, and 0.4 μg/cm^2 PC/PE/CL (2:1:1) mixture were required to ensure a condensed lipid monolayer at the surface of the electrolyte, i.e., an aqueous solution containing 0.05 M NaCl and 20 mM Tris-HCl at pH 7.4. Oxygen was displaced from the solution by argon, and equilibrium between the bulk and the surface layer was facilitated by gently stirring the subphase. The starting potential was chosen in the stable region of the monolayer, i.e., at −0.2 V.

PM-IRRAS measurements

Interface studies of mtCK in the presence or absence of lipid monolayers were performed by means of PM-IRRAS measurements as elsewhere described (43–46). The spectra were recorded on a Nicolet Nexus 870 Fourier transform infrared spectrometer (Thermo Scientific, Madison, WI). The light beam was reflected toward the optical bench by a mobile mirror. It was then polarized by a ZnSe polarizer and directed toward a photoelastic modulator that modulated the beam between a parallel (p) and perpendicular (s) polarization. The light beam was directed toward the monolayer at an angle of 75° and reflected on a photovoltaic MCT-A detector cooled at 77 K. The detected signal was then processed to obtain the differential reflectivity spectrum:

$$\Delta R/R = J_2 \times \left(R_p - R_s\right)/\left(R_p + R_s\right),$$

where J_2 is the Bessel function, which depends only on the photoelastic modulator, and R_s and R_p are the parallel and perpendicular reflectivities, respectively. To remove the Bessel function contribution, as well as that of the water absorption, the monolayer spectrum was divided by that of

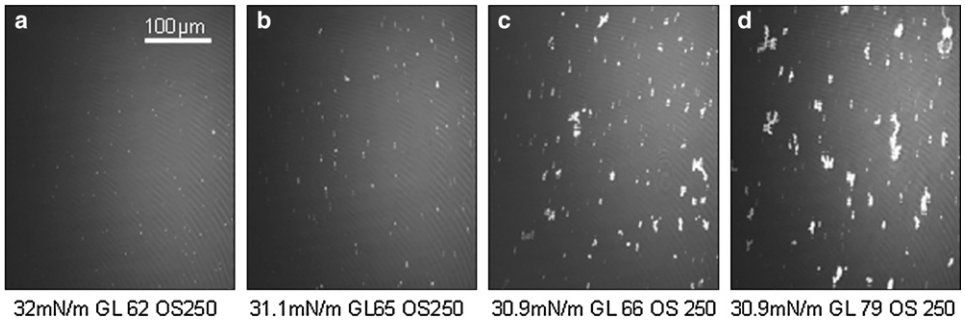

FIGURE 1 BAM images of a PC/PE/CL (2:1:1) monolayer before mtCK injection (*a*) and 20 min (*b*), 60 min (*c*), and 140 min (*d*) after mtCK injection. Lateral surface pressure, gray level (GL), and obturation speed (OS) are indicated below each image.

the pure subphase. Then 1024 scans were added at a resolution of 8 cm^{-1} for pure mtCK, pure lipid monolayers, or lipid monolayers in the presence of mtCK. To obtain the spectra of lipid-bound mtCK, the spectra of the pure lipids were subtracted from those of the mixed monolayers. Each presented spectrum is the resulting average of at least three independent experiments. Each experiment consisted of three series of scans. The mean angle distribution of the dipole moments of α-helices were calculated using the Protein Dipole Moments Server (47).

RESULTS

MtCK interaction with a monolayer mimicking the composition of the inner mitochondrial membrane

A phospholipid mixture of PC, PE, and CL in a 2:1:1 molar ratio, mimicking the composition of the inner mitochondrial membrane, was spread at the air-buffer interface at ~30 mN/m lateral surface pressure. BAM images of the pure PC/PE/CL monolayer showed a rather homogeneous surface (Fig. 1 *a*). The average gray level of the images remained constant at a value of 62 for an obturation speed (OS) of 250 s^{-1}. Using a refractive index of 1.46 for the lipid monolayer, the average gray level of the images permitted us to estimate an apparent average film thickness of 1.8 nm for the lipid mixture at 30 mN/m, compatible with the thickness of one membrane leaflet. MtCK was injected beneath the monolayer at a final concentration of 4 nM, corresponding to a 12:1 CL/mtCK molar ratio. No increase in the lateral surface pressure was recorded. Nevertheless, ~20 min after protein injection, bright domains began to appear at the interface and progressively increased in number and in size (Fig. 1, *b–d*); 140 min after protein injection, the average global film thickness increased from 1.8 to 2.4 nm. The gray level locally measured on the bright areas of the image (Fig. 1 *d*) permitted us to estimate a local thickness attaining 10 nm for the formed clusters. The clustering effect was visible for CL/mtCK molar ratios ranging from 33:1 to 3:1, corresponding to protein concentrations in the subphase of 0.5–16 nM. In the absence of protein, the overall aspect of the monolayer did not significantly vary for the duration of the experiment. This was the case for all lipids tested.

Lipid cluster formation required the presence of negatively charged CL

To investigate whether these bright domains were dependent on a specific phospholipid, mtCK was injected beneath monolayers containing either only the zwitterionic PC or the anionic CL, pure or in a PC/CL (3:1) mixture. For each lipid system tested, the initial lateral surface pressure was ~30 mN/m. Before protein injection, whatever the tested monolayer, no bright domains were observed at the interface (Fig. 2 *a*), and considering a refractive index of 1.46, the average film thickness was estimated between 1.8 nm and 2 nm. Images recorded after protein injection showed no modification of the monolayer of pure PC, and no increase in the average gray level was recorded (Fig. 2, *PC panels*). The estimated thickness of the monolayer apparently was unaffected by the presence of mtCK. Different observations were made with anionic monolayers. Indeed, before mtCK injection, the PC/CL (3:1) monolayer appeared as a homogeneous surface (Fig. 2 *a*, PC:CL). However, 15–20 min after protein injection, domains appeared and then slightly increased in size with time (Fig. 2, *b–d*, PC/CL). They were smaller than those observed with the PC/PE/CL (2:1:1) monolayer and their increase was more limited; thus, monolayer morphology upon mtCK binding may be influenced by the presence of PE. The gray level became more intense, indicating a rise in the average thickness. On a pure CL monolayer, the spots were seen at about the same time, but their number increased more rapidly. The images recorded 20 min after protein injection showed a large number of bright spots (Fig. 2 *b*, *CL panel*). Their size increased with time (Fig. 2, *c* and *d*, *CL panels*), forming large patches, indicating that MtCK could more easily recruit CL molecules. The average global thickness of the film increased from 2 to 2.8 nm in 140 min, a stronger increase than the one observed with a PC/PE/CL (2:1:1) or PC/CL (3:1) monolayer, probably due to a higher amount of mtCK concentrated at the interface by the 100% negatively charged CL monolayer. For all of the CL-containing monolayers tested, mtCK induced a thickening of the film, but also the formation of high-reflectivity regions.

Structural models of mtCK binding to CL, deduced from BAM pictures

As mentioned above, on a pure CL monolayer no spots were observed before mtCK injection (Fig. 3*a A*); however, the addition of mtCK induced the formation of bright aggregates of different sizes but of characteristic fractal shape (Fig. 3 *a*,

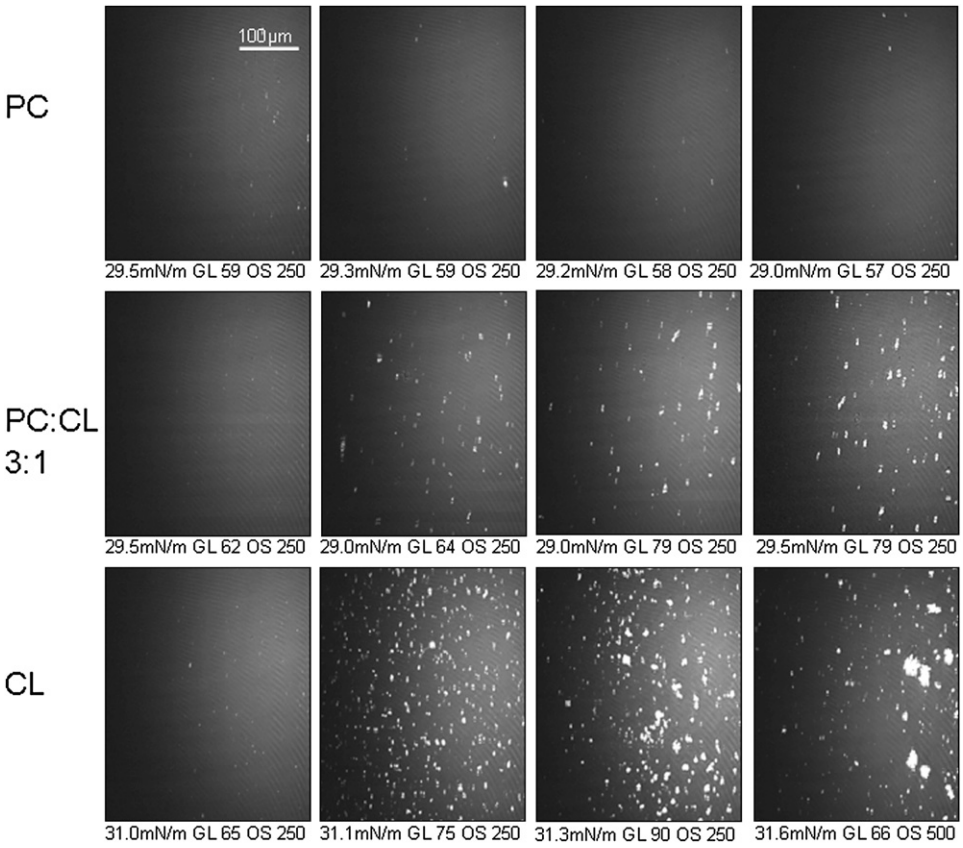

FIGURE 2 BAM images of PC (*top*), PC/CL (3:1) (*middle*), and CL (*bottom*) monolayers before mtCK injection (*a*) and 20 min (*b*), 60 min (*b*), or 120 min (*d*) after mtCK injection. Lateral surface pressure, GL, and OS are indicated below each image.

B–D). The film thickness profile was calculated along the white line in image *D* of Fig. 3 *a*. A global increase was observed on the whole length of the image, with maximum values around 12 nm, corresponding to the bright regions observed on the image (Fig. 3 *a*, *inset*). Based on the brightness of the BAM pictures indicating changes in the reflectivity at the interface, the apparent thickness of the interfacial film was modeled at each point of the BAM picture. Different views of the CL monolayer in the presence and absence of mtCK were reconstituted (Fig. 3 *b*). The aspect of a pure CL membrane (Fig. 3 *b*, *A* and *B*) was homogeneous, with a maximum thickness of 1.9 nm, as expected for one membrane leaflet, indicating that CL adopted a monolayer organization. In the presence of mtCK the interfacial film was irregular, with a maximum thickness of 12 nm (Fig. 3 *b*, *C–E*).

Effects of mtCK on the differential capacity of monolayers with and without CL

To delineate the perturbations that occur in a membrane after mtCK interaction, the differential capacity (C) of a hanging mercury drop electrode in direct contact with a condensed phospholipid monolayer was recorded in the presence or absence of protein. Fig. 4 *a* (*solid line*) describes the evolution of C of a pure condensed CL monolayer for a potential varying between −0.2 and −1.4 V (C versus E curve). Around the potential of zero charge of the electrode (pzc) (−0.45 V Ag/AgCl sat. KCl), the value of C was stable and constant over a wide potential range between −0.2 V and −0.7 V. This value of C, ~1.5 μF/cm^2, is characteristic of a condensed phospholipid monolayer (42,48). Moreover, slight potential variation around the pzc did not significantly modify the condensed monolayer. Indeed, when we superimposed a 0.2 V potential (in the range of the 0.14 V mitochondrial membrane potential (49,50)) on both sides of the pzc, C remained constant. At more negative potential (−0.9 V to −1.4 V), two main peaks appeared.

MtCK addition beneath the CL monolayer induced an increase in the differential capacity in the −0.2 V to −0.9 V region (Fig. 4 *a*, *dotted line*). Between −0.9 V and −1.4 V, the shape of the peaks observed for the pure phospholipid was severely altered and their height distinctly decreased.

For a pure condensed PC monolayer (Fig. 4 *b*, *solid line*), C was constant and stable between −0.2 V and −0.7 V, indicating that a condensed state was achieved. Two main peaks between −0.9 V and −1.4 V were observed. Their presence in this region was previously reported (48,51). The presence of mtCK induced no increase in C in the −0.2 V to −0.7 V potential range (Fig. 4 *b*, *dotted line*). The shape of the peaks observed at more negative potential varied only slightly.

The PC/PE/CL (2:1:1) mixture also showed a stable value of the differential capacity in a wide potential range around the

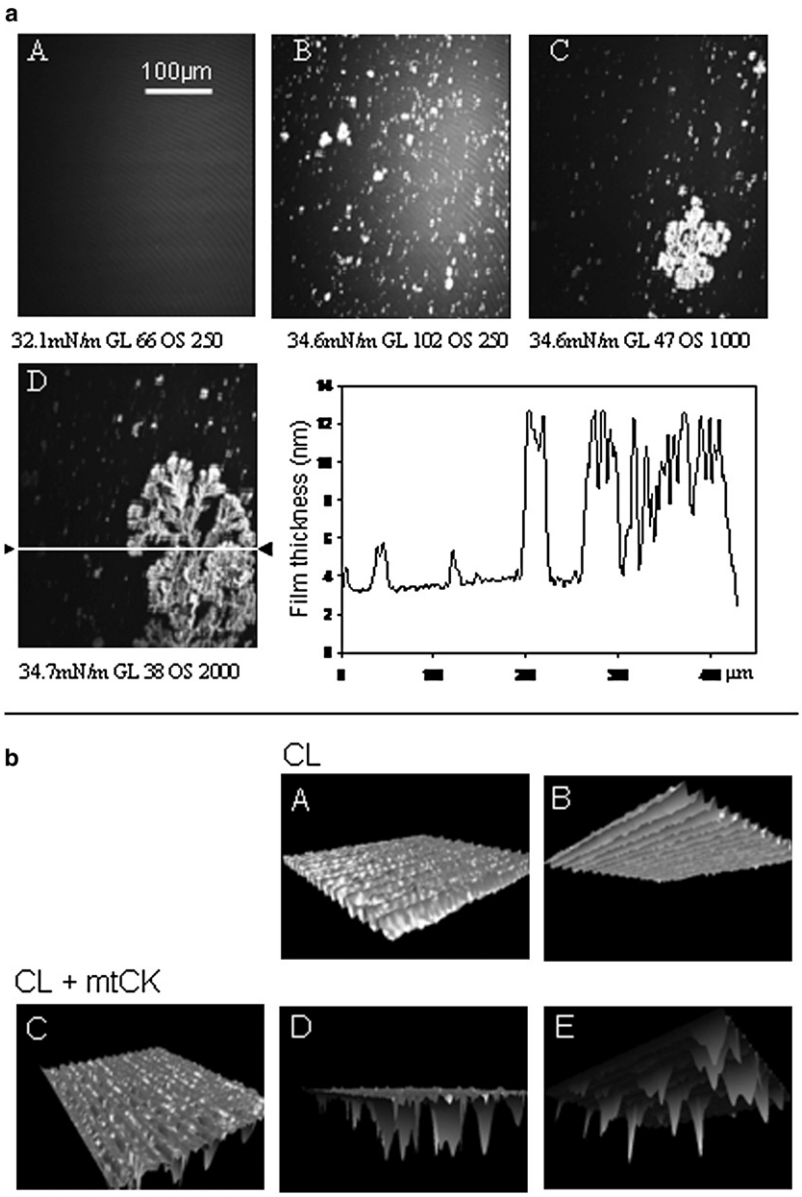

FIGURE 3 (*a*) BAM images of a CL monolayer before mtCK injection (*A*) and 3 h (*B*) or 3 h 30 min (*C* and *D*) after mtCK injection. Lateral surface pressure, GL, and OS are indicated below each image. (*Inset*) Film thickness profile along the white line in image *D*. (*b*) Theoretical 3D simulation of a CL monolayer in the absence (*top*) and presence (*bottom*) of mtCK (3D views of images *A* and *D* from Fig. 3 *a*). (*A*) Top and (*B*) bottom views of a pure CL monolayer. (*C*) Top, (*D*) side, and (*E*) bottom views of a CL-mtCK monolayer.

pzc (Fig. 4 *c*, *solid line*). In the PC/PE/CL (2:1:1) mixture, the characteristic peaks of the constituting lipids merged in a wide feature, with a maximum value at −1.2 V and shoulders around −1 V and −1.3 V. After mtCK injection, the differential capacity in the −0.2 V to −0.9 V region increased (Fig. 4 *c*, *dotted line*). At more negative values of the potential, the wide feature observed for the pure lipid mixture was modified and three distinct peaks appeared.

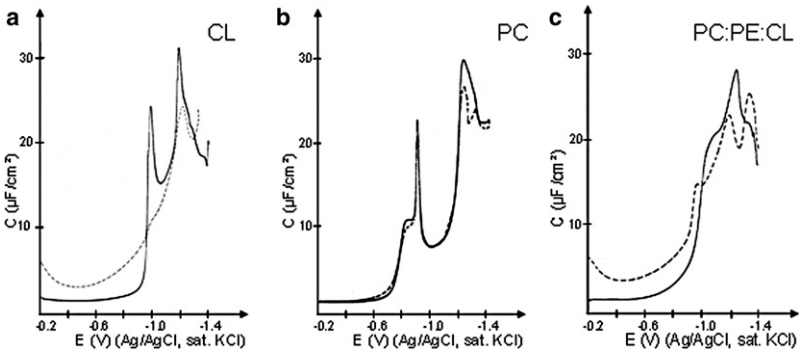

FIGURE 4 Differential capacity versus potential curves obtained with a hanging mercury drop electrode in contact with a condensed CL (*a*), PC (*b*), or PC/PE/CL (2:1:1) (*c*) monolayer before (*solid lines*) and after (*dotted lines*) addition of mtCK at 4 nM final concentration in the supporting electrolyte.

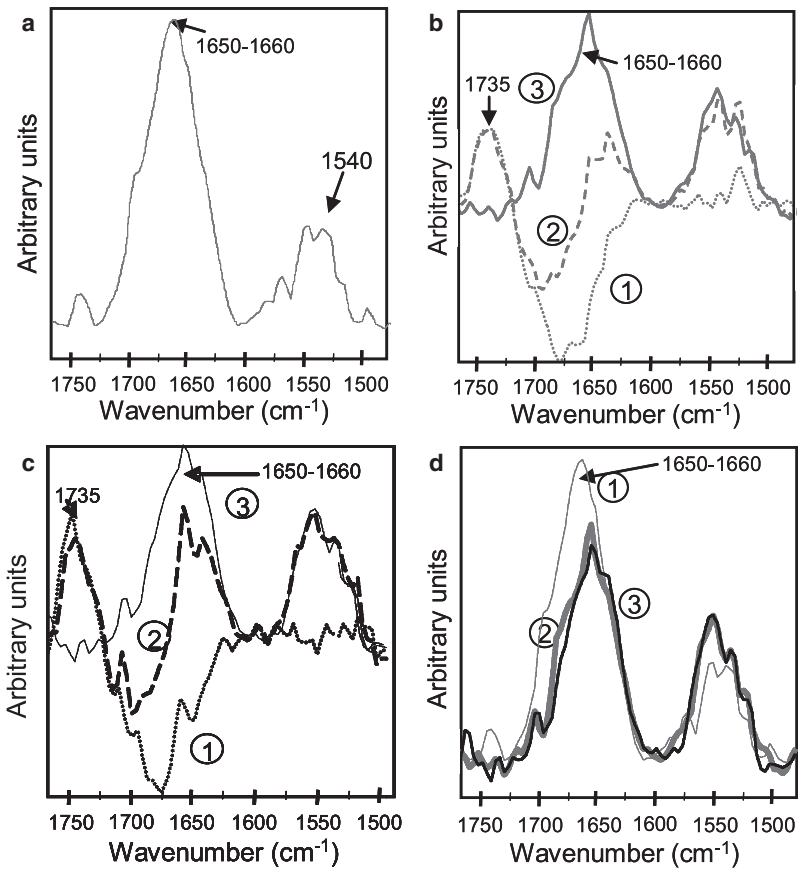

FIGURE 5 PM-IRRAS spectra. (*a*) MtCK at the air-buffer interface (*thin gray curve*). (*b*) CL monolayer in the absence (dotted gray curve 1) and in the presence of mtCK (*dashed gray curve 2*), difference spectrum of mtCK (i.e., CL in the presence of mtCK minus CL) (*bold gray curve 3*). (*c*) PC/PE/CL (2:1:1) monolayer in the absence (*dotted black curve 1*) and presence (*dashed black curve 2*) of mtCK, and difference spectrum of mtCK (i.e., PC/PE/CL (2:1:1) in the presence of mtCK minus PC/PE/CL (2:1:1)) (*bold black curve 3*). (*d*) Spectrum of mtCK at the air-buffer interface (*thin gray curve 1*) and difference spectra of mtCK at the CL or PC/PE/CL (2:1:1) buffer interface (*bold gray curve 2* and *bold black curve 3*, respectively); the overlaid spectra correspond to curve 1 in *a* and curve 3 in *b* and *c*, and are presented on a common scale.

Protein orientation at the interface in the absence and presence of negatively charged phospholipids

The ability of mtCK molecules to form a layer at the air-buffer interface (52) allowed us to investigate the protein conformation and orientation in the absence of lipids. The PM-IRRAS spectrum of a pure mtCK film at the air/buffer interface (Fig. 5 *a*) exhibited a strong positive amide-I band located at 1659 cm^{-1}, characteristic of the presence of α-helical structures, and a lower amide-II band at 1545 cm^{-1} (53). The behavior of mtCK in interaction with a CL-containing monolayer at a lateral surface pressure of ~30 mN/m was then investigated. Subtraction of the pure lipid spectra from the mixed mtCK-lipid spectra permitted us to distinguish the characteristic contribution of the protein (Fig. 5, *b* and *c*). The MtCK spectrum in the presence of a CL or a PC/PE/CL (2:1:1) monolayer showed a large amide-I band centered around 1651 cm^{-1}. Isotropic water vapor was compensated for by modulating polarized infrared light, and contributed very little to the noise. The poor signal/noise ratio of PM-IRRAS spectra comes from the intrinsic weak-intensity signals combined with surface sensitivity to external vibration. Although three independent measurements were made and averaged, subtraction of the liquid-water band (i.e., interfacial water molecules interacting with phospholipids that were displaced by mtCK adsorption and phospholipid rearrangements) can contribute to the experimental errors, especially by shifting the amide-I band. PM-IRRAS spectra are sensitive to both protein-domain orientation and conformational change, in contrast to unpolarized infrared spectra, which are sensitive only to the conformational changes. In this respect, unpolarized infrared transmittance spectra indicate that the conformational changes of mtCK induced by its interaction with liposomes are relatively weak (14). Therefore, we assumed that the secondary structure changes contribute very little to the changes in the PM-IRRAS spectra.

The amide-I/amide-II absorbance ratio measured on the PM-IRRAS spectrum can be taken as an approximate measure of the relative orientation of the amide groups associated with a class of protein secondary structures (43,46). We hypothesized that the intensity of the amide-I band at 1659 cm^{-1} reflected mostly the α-helices and neglected the contribution of other secondary structures. Indeed, the mean orientation of β-sheet and random coil structures could not be calculated since the position of their band components is not well resolved and cannot be determined with accuracy. The amide-I/amide-II ratio of 3.2 measured on the mtCK PM-IRRAS spectrum suggested a global orientation of the α-helices between 25° and 30° with respect to the interface plane, according to simulation models (46). The

amide-I/amide-II ratio diminished from 3.2 in the absence of lipids to 1.6 in the presence of a CL-containing monolayer (Fig. 5 *d*). According to simulation models (46), this value indicated a global orientation of the α-helices tilted from the interface plane by 45°.

DISCUSSION

Three complementary techniques were used to obtain a thorough characterization of the mtCK interaction with a phospholipid monolayer formed at the air-buffer interface: BAM, a.c. polarography, and PM-IRRAS. BAM permits visualization of the film morphology, whereas a.c. polarography characterizes the protein interaction with a condensed lipid monolayer at the buffer surface and determines the stability of the monolayer relative to variations of the potential. PM-IRRAS monitors modifications in the conformation and the orientation of the protein upon membrane binding.

Topology and apparent thickness of PC/PE/CL (2:1:1) phospholipid monolayers containing mtCK, deduced from BAM images

Because of their ability to self-assemble at the air-water interface, phospholipid monolayers constitute a suitable experimental model for characterizing the interaction between peripheral proteins and membranes (54). The mitochondrial inner membrane consists mainly of PC, PE, and CL in a 2:1:1 molar ratio, characterized by a high percentage of unsaturated fatty acids (>50% for PC and PE, and >80% for CL) and a high proportion of C18 chains (>50% for PC and PE, and 83% for CL) (55,56). A PC/PE/CL (2:1:1) monolayer served to model the mitochondrial membrane. This monolayer was visualized by BAM and showed a rather homogeneous surface at a resolution of 2 μm (Fig. 1 *a*). Because of the highly unsaturated fatty acids, the phospholipid film at the interface was fluid. An average thickness of 1.8 nm was estimated. When injected beneath this monolayer, mtCK induced a time-dependent phospholipid clustering (Fig. 1, *b–d*). The domains gradually increased in size and adopted irregular shapes. Simultaneously, a global rise of the gray level was recorded corresponding to an increase in the calculated average thickness. Thus, the average thickness increased from ~1.8–2.4 nm due to accumulation of mtCK molecules at the buffer-lipid interface. This value is lower than the dimensions of the mtCK octamer (9.3 × 9.3 × 8.6 nm) (57), indicating an inhomogeneous surface distribution of the enzyme. Of interest, a thickness of ~10 nm, compatible with the height of the protein-lipid complex but 5–6 times greater than that of the pure monolayer, was locally measured at the bright regions (Fig. 1 *d*). Such an increase cannot be explained only by pure lipid clustering, even taking into account a possible condensation and a consequent increase in the lipid refractive index. This points to the formation of a lipid-protein complex. Alternatively, since mtCK accumulates at the air-buffer interface in the absence of phospholipids (52), a question may arise as to whether the observed bright areas were due to protein-protein complexes coadsorbed at the interface. However, at similar surface pressure, no domains were visible on a monolayer of pure PC (Fig. 2). This indicates that, at this lateral surface pressure, mtCK cannot reach the air-buffer interface. Moreover, protein intercalated between lipids should induce a large increase in the lateral surface pressure. The lateral surface pressure does not increase for the PC/PE/CL (2:1:1) mixture and increases only marginally (3 mN/m) for the CL monolayer. Thus, the insertion of protein molecules between lipids is limited and probably involves only some domains of the molecule. All of these findings indicate that the observed clusters were composed of protein-CL complexes.

The clustering effect of mtCK on a pure CL monolayer was enhanced compared to that on monolayers containing 25% CL (Fig. 2), as the bright spots drastically increased in number and size and adopted large fractal shapes several hours after injection (Fig. 3 *a*). These findings indicate that the observed clusters were composed of protein-CL complexes. Their particular shape is probably due to a high line tension between the clusters and the embedding fluid environment, indicating a gel-fluid phase separation (58).

Protein insertion into the monolayers as evidenced by differential capacity measurements

Complementary information on the perturbations induced by protein binding to membranes can be obtained by measuring the differential capacity of a mercury electrode in direct contact with a condensed monolayer upon protein interaction (42). This method permits one to assess whether a water-soluble molecule interacts with a condensed lipid monolayer by simple adsorption at the charged polar head or whether the binding involves insertion into the monolayer. The differential capacity of the interface varies with the potential imposed between the working and the reference electrodes, and depends on the type of molecules in contact with the mercury electrode.

Measurements were taken around the potential of zero charge of the electrode (pzc) (−0.45 V), where there is no or negligible superimposed electric field that could affect the interaction. The highest value of C corresponds to the pure electrolyte. When a molecule (protein or phospholipid) adsorbs on the electrode, C decreases. A condensed state at the electrode is achieved when the adsorbed molecules form a compact layer at the interface and no electrolyte molecules are in contact with the electrode. For a condensed phospholipid monolayer, since the hydrophobic chains adsorbed at the electrode have a low dielectric constant, the value of C is low over a wide potential range including the pzc. The value of C is higher for proteins adsorbed at the electrode as single species than for phospholipids. The addition of mtCK beneath the condensed CL monolayer induced a significant increase in C around the pzc (Fig. 4 *a*),

indicating a perturbation of the continuity of the dense phospholipid layer and, consequently, a certain degree of protein insertion into the monolayer (42,51). However, no increase was observed when the protein was injected beneath a zwitterionic PC monolayer, indicating that no insertion occurred (Fig. 4 *b*). Because insertion into the monolayer is generally associated with hydrophobic interactions, this further supports the previous hypothesis that mtCK binding to membranes involves both electrostatic and hydrophobic components (10). The peak observed at −1.0 V on the *C* versus *E* curve may be attributed to rearrangements of the CL monolayer in response to potential variations, as was proposed in the case of PC (59). At this potential, the monolayer, which is normally oriented with the acyl chains toward the electrode and the polar headgroup toward the buffer subphase, is destabilized and a competition takes place at the electrode between the polar heads and the acyl chains. The fine shape of the peak indicates that rearrangements occurred rapidly. In the presence of mtCK the height of the peak decreased. From an electrochemical kinetic point of view, a slower rearrangement process occurred at the electrode, meaning that the protein-containing monolayer was less disturbed by potential variations. Thus, the addition of mtCK modified the monolayer properties, indicating that the protein-lipid complex stabilized the monolayer. The addition of mtCK beneath a PC/PE/CL (2:1:1) monolayer resulted in an increase in the differential capacity in the −0.2 to −0.7 V region (Fig. 4 *c*). As in the case of the CL monolayer, this indicates a certain degree of protein insertion into the monolayer. At more negative potential values, for the pure lipid mixture in the absence of protein, the characteristic peaks of each individual lipid were not distinct and they merged into a wide peak, with a maximum value at −1.2 V and shoulders at −1 V and −1.3 V. In the presence of mtCK, the wide peak was resolved in three distinct components. As in the case of the CL monolayer, two peaks were observed around −1 V and −1.2 V, which can be attributed to the specific effect of the protein on CL, since the specific peaks of PC (Fig. 4 *b*) or PE (39) are below −0.9 V. The binding of mtCK to the PC/PE/CL (2:1:1) monolayer resulted in the appearance of the characteristic peaks of CL, at −1V and −1.2 V, indicating segregation of CL from the remaining other lipids. These findings can be related to the lipid segregation observed on the BAM images.

Average orientation changes of mtCK structural elements upon monolayer binding

To monitor the conformational and orientation changes that occurred upon mtCK binding to a negatively charged phospholipid monolayer, PM-IRRAS spectra of the protein were recorded in the absence and presence of lipids. Earlier fluorescence and unpolarized infrared transmittance measurements indicated no major conformational changes of mtCK upon binding to liposomes (14), suggesting that PM-IRRAS spectra reveal mostly changes in the mean orientation of transition dipole moments, reflecting protein domain movements. Although the PM-IRRAS amide-I band shifted from 1659 cm^{-1} to 1651 cm^{-1} upon lipid binding, the shift was not assigned to secondary structure changes, but rather to a redistribution of amide-I component bands reflecting protein-domain movements and/or artifacts caused by subtractions. This is corroborated by changes in the amide-I/amide-II intensity ratio that are too large to be assigned to secondary structure changes only. Despite the poor signal/noise ratio and the eventual errors caused by the subtraction, the intensity changes in the amide-I/amide-II ratio were significant and indicated that the mean orientation of the structural components was modified. We hypothesized that the peak position reflected the main structural component by neglecting the other contributions. Therefore, the mean peak at ~1659–1651 cm^{-1} essentially reflected α-helical structures. Since the contribution of β-sheet structures to PM-IRRAS spectra cannot be accurately determined, we did not attempt to calculate their mean orientations. Using a simulation model correlating the orientation of α-helical structures and the amide-I/amide-II ratio (46), we found that in the absence of lipids the global dipole moment of α-helices was tilted by 30° with respect to the interface plane. In the absence of a rabbit mtCK structure, the chicken mtCK structure served as a structural model (57). Chicken and rabbit mtCK structures have a high degree of sequence similarity and both exist either as membrane-binding octamers or as dimers (12). At the air-buffer interface, the orientation of the octamer that best agrees with the global tilt of 30° is the one in which the top and bottom faces are in a plane parallel to the surface (Fig. 6). In this case, the two longest α-helices (α12 E341-E363 and α9 M241-R262), as well as most of the small ones, are only slightly tilted from the interface plane, although several helices, such as α6 R143-A158 and α7 E176-D184, have a vertical orientation. The global orientation of the dipole moment of α-helices estimated from Protein Dipole Moment Server (47) was 29° with respect to the surface plane. The amide-I/amide-II ratio diminishes from 3.2 in the absence of lipids to 1.6 for CL-containing monolayers (Fig. 5). We attributed the drastic decrease in the amide-I/amide-II ratio to a reorientation of one or several α-helix structures, corresponding to an apparent tilt in the helices' orientation from 25–30° (absence of lipids) to 45° (presence of lipids) with respect to the interface plane. A similar phenomenon—a reorientation of the α-helix from a parallel toward a more perpendicular position with respect to the surface upon interaction with a lipid monolayer—has been observed for human annexin A6 (60). In the case of mtCK, the 22-residues-long C-terminal α-helix (α12) is a candidate for such a change. Its position near the lipid-binding site makes it likely to be sensitive to mtCK fixation to lipids. The dipole moment of the C-terminal α-helix is rather large compared to that of the other helices, so any modification of its orientation might

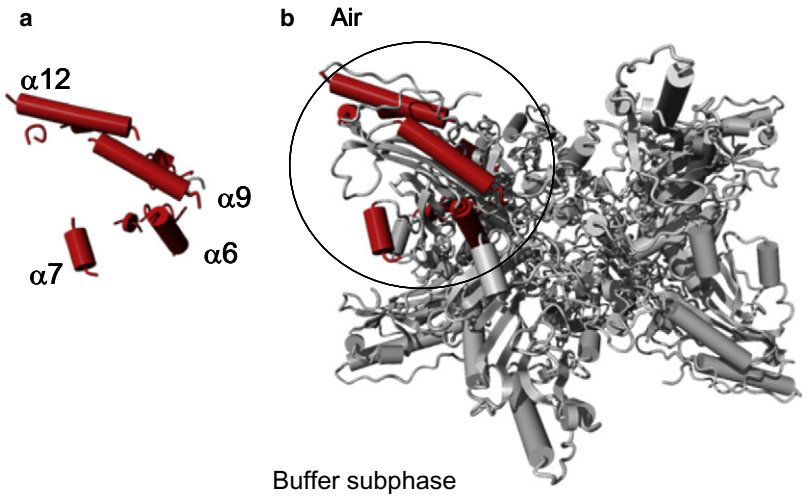

FIGURE 6 Proposed orientation of mtCK monomer α helices (*a*) and the corresponding side view of the mtCK octamer (*b*) at the air-buffer interface. (*Red*) α-Helices of one mtCK monomer corresponding to the orientation represented in Fig. 7 *a*. The proposed orientation of the octamer at the air-buffer interface is with the top and bottom faces parallel to the interface plane. The top and bottom faces of the octamer are identical and contain the lipid-binding sites.

have a significant impact on the orientation of the dipole moment of the whole molecule. The protein binding might induce a reorientation of this helix toward a more vertical position. In this new configuration, the positively charged Arg^{364} (rabbit mtCK)/Lys^{364} (chicken mtCK) residue, located at the extremity of the α12 helix, would find itself oriented toward the monolayer and might thus participate in the membrane binding. It has been shown that this helix interacts with the neighboring α11 helix in the cytosolic isoform, MMCK (61). Since this isoenzyme has a high degree of structural similarity with its mitochondrial counterpart, we can tentatively suggest that the change in the orientation of the α12 helix induces a perturbation of the α11 helix and other vicinal structures so that the relative position of the N- and C-terminal domain of the monomer is modified. We can hypothesize that the top monomers, which directly face the lipid polar heads, might be more affected by the presence of charged lipids than the bottom monomers. This would result in a tilt of the resultant α-helix dipole moment from 30° with respect to the interface plane (Fig. 7 *a*) toward a more vertical position (Fig. 7 *b*). The deviation from the symmetry of the molecule could reflect the change in the mean orientation of the experimentally observed helices.

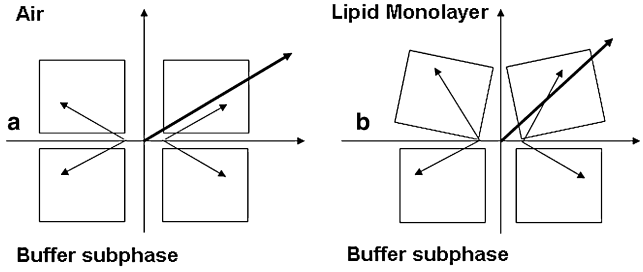

FIGURE 7 Proposed arrangement of mtCK octamer at the air-buffer interface (*a*) and after interaction with a phospholipid monolayer (*b*, *side view*). Small arrows indicate the estimated orientation of the monomers' dipole moments; large arrows represent the resulting dipole moment of the whole molecule.

CONCLUSIONS

The membrane association of the mtCK octameric form is a key determinant of both its enzymatic function (62) and its structural role in ensuring mitochondrial structure and morphology (6–8). Located in the mitochondrial intermembrane space in high concentration at the contact points (63), this enzyme may facilitate the contact between the inner and outer membranes (64). Beutner et al. (65) suggested that the presence of octameric mtCK at contact sites prevents direct interaction between the voltage-dependent anion channel (VDAC) and ANT, and thus opening of the mitochondria permeability transition pore. Several of the proteins that participate in the formation of lipid/protein complexes at the mitochondrial contact sites (ANT, cytochrome *c*, and tBid) show, as is the case for mtCK, a high affinity for CL (21,66–70). Therefore, CL could be one of the factors that mediate the formation of such lipid/protein complexes. Several recent reports have related this phospholipid to apoptotic phenomena. It has been suggested that this molecule has a role in maintaining cytochrome *c* ''anchored'' at the inner membrane, and controlling the amount that can be released during apoptosis (67,68). Another role is related to its affinity for one of the essential regulators of the release of proapoptotic factors into the cytosol, tBid (69,70). The interaction of tBid with the outer membrane of the mitochondria triggers Bax insertion into the membrane, as well as its oligomerization and, consequently, pore formation. Therefore, any modification in CL distribution in the membrane could influence some of the apoptosis-triggering events. Our findings show that mtCK induces the formation of domains enriched in CL on biomimetic monolayers. Moreover, the uniform aspect of the monolayers before mtCK injection and the slow growth of the clusters indicate that the protein did not bind to self-associated CL aggregates but was able to recruit phospholipid molecules. MtCK-lipid interaction was accompanied by protein domain movements, as well as insertion into the phospholipid monolayer,

pointing to an overall stabilization of the biomimetic membrane. Because of the high amount of mtCK present in the intermembrane space, the lipid segregation induced by this enzyme may participate in the modulation of CL availability to bind other proteins, such as cytochrome *c*, other electron-carrier proteins, proteins of the Bcl-2 family, and ANT, and thus regulate essential stages in energy homeostasis or apoptosis.

We thank Dr. J. Clavilier for helpful discussions and suggestions, and Dr. J. Carew for correcting the English.

REFERENCES

1. Wallimann, T., M. Wyss, D. Brdiczka, K. Nicolay, and H. M. Eppenberger. 1992. Intracellular compartmentation, structure and function of creatine kinase isoenzymes in tissues with high and fluctuating energy demands—the phosphocreatine circuit for cellular energy homeostasis. *Biochem. J.* 281:21–40.
2. Nicolay, K., M. Rojo, T. Wallimann, R. Demel, and R. Hovius. 1990. The role of contact sites between inner and outer mitochondrial membrane in energy transfer. *Biochim. Biophys. Acta.* 1018:229–233.
3. Dolder, M., S. Wendt, and T. Wallimann. 2001. Mitochondrial creatine kinase in contact sites: interaction with porin and adenine nucleotide translocase, role in permeability transition and sensitivity to oxidative damage. *Biol. Signals Recept.* 10:93–111.
4. Brdiczka, D., G. Beutner, A. Ruck, M. Dolder, and T. Wallimann. 1998. The molecular structure of mitochondrial contact sites. Their role in regulation of energy metabolism and permeability transition. *Biofactors.* 8:235–242.
5. O'Gorman, E., G. Beutner, M. Dolder, A. P. Koretsky, D. Brdiczka, et al. 1997. The role of creatine kinase in inhibition of mitochondrial permeability transition. *FEBS Lett.* 414:253–257.
6. Speer, O., N. Back, T. Buerklen, D. Brdiczka, A. Koretsky, et al. 2005. Octameric mitochondrial creatine kinase induces and stabilizes contact sites between the inner and outer membrane. *Biochem. J.* 385:445–450.
7. Dolder, M., B. Walzel, O. Speer, U. Schlattner, and T. Wallimann. 2003. Inhibition of the mitochondrial permeability transition by creatine kinase substrates. Requirement for microcompartmentation. *J. Biol. Chem.* 278:17760–17766.
8. Lenz, H., M. Schmidt, V. Welge, T. Kueper, U. Schlattner, et al. 2007. Inhibition of cytosolic and mitochondrial creatine kinase by siRNA in HaCaT- and HeLaS3-cells affects cell viability and mitochondrial morphology. *Mol. Cell. Biochem.* 306:153–162.
9. Schlame, M., and W. Augustin. 1985. Association of creatine kinase with rat heart mitochondria: high and low affinity binding sites and the involvement of phospholipids. *Biomed. Biochim. Acta.* 44: 1083–1088.
10. Schlattner, U., F. Gehring, N. Vernoux, M. Tokarska-Schlattner, D. Neumann, et al. 2004. C-terminal lysines determine phospholipid interaction of sarcomeric mitochondrial creatine kinase. *J. Biol. Chem.* 279:24334–24342.
11. Schlegel, J., B. Zurbriggen, G. Wegmann, M. Wyss, H. M. Eppenberger, et al. 1988. Native mitochondrial creatine kinase forms octameric structures. Isolation of two interconvertible mitochondrial creatine kinase forms, dimeric and octameric mitochondrial creatine kinase: characterization, localization, and structure-function relationships. *J. Biol. Chem.* 263:16942–16953.
12. Marcillat, O., D. Goldschmidt, D. Eichenberger, and C. Vial. 1987. Only one of the two interconvertible forms of mitochondrial creatine kinase binds to heart mitoplasts. *Biochim. Biophys. Acta.* 890:233–241.
13. Rojo, M., R. Hovius, R. Demel, T. Wallimann, H. M. Eppenberger, et al. 1991. Interaction of mitochondrial creatine kinase with model membranes. A monolayer study. *FEBS Lett.* 281:123–129.
14. Granjon, T., M. J. Vacheron, C. Vial, and R. Buchet. 2001. Mitochondrial creatine kinase binding to phospholipids decreases fluidity of membranes and promotes new lipid-induced β structures as monitored by red edge excitation shift, laurdan fluorescence, and FTIR. *Biochemistry.* 40:6016–6026.
15. Granjon, T., M. J. Vacheron, R. Buchet, and C. Vial. 2003. Mg-nucleotides induced dissociation of liposome-bound creatine kinase: reversible changes in its secondary structure and in the fluidity of the bilayer. *Mol. Membr. Biol.* 20:163–169.
16. Krebs, J. J., H. Hauser, and E. Carafoli. 1979. Asymmetric distribution of phospholipids in the inner membrane of beef heart mitochondria. *J. Biol. Chem.* 254:5308–5316.
17. Ardail, D., J. P. Privat, M. Egret-Charlier, C. Levrat, F. Lerme, et al. 1990. Mitochondrial contact sites. Lipid composition and dynamics. *J. Biol. Chem.* 265:18797–18802.
18. Eble, K. S., W. B. Coleman, R. R. Hantgan, and C. C. Cunningham. 1990. Tightly associated cardiolipin in the bovine heart mitochondrial ATP synthase as analyzed by 31P nuclear magnetic resonance spectroscopy. *J. Biol. Chem.* 265:19434–19440.
19. Fry, M., and D. E. Green. 1981. Cardiolipin requirement for electron transfer in complex I and III of the mitochondrial respiratory chain. *J. Biol. Chem.* 256:1874–1880.
20. Fry, M., and D. E. Green. 1980. Cardiolipin requirement by cytochrome oxidase and the catalytic role of phospholipid. *Biochem. Biophys. Res. Commun.* 93:1238–1246.
21. Nury, H., C. Dahout-Gonzalez, V. Trezeguet, G. J. Lauquin, G. Brandolin, et al. 2006. Relations between structure and function of the mitochondrial ADP/ATP carrier. *Annu. Rev. Biochem.* 75:713–741.
22. Gonzalvez, F., and E. Gottlieb. 2007. Cardiolipin: setting the beat of apoptosis. *Apoptosis.* 12:877–885.
23. Degroote, S., J. Wolthoorn, and G. van Meer. 2004. The cell biology of glycosphingolipids. *Semin. Cell Dev. Biol.* 15:375–387.
24. Mileykovskaya, E., and W. Dowhan. 2000. Visualization of phospholipid domains in *Escherichia coli* by using the cardiolipin-specific fluorescent dye 10-N-nonyl acridine orange. *J. Bacteriol.* 182: 1172–1175.
25. Kawai, F., M. Shoda, R. Harashima, Y. Sadaie, H. Hara, et al. 2004. Cardiolipin domains in *Bacillus subtilis* marburg membranes. *J. Bacteriol.* 186:1475–1483.
26. Zhang, M., E. Mileykovskaya, and W. Dowhan. 2002. Gluing the respiratory chain together. Cardiolipin is required for supercomplex formation in the inner mitochondrial membrane. *J. Biol. Chem.* 277:43553–43556.
27. Zhang, M., E. Mileykovskaya, and W. Dowhan. 2005. Cardiolipin is essential for organization of complexes III and IV into a supercomplex in intact yeast mitochondria. *J. Biol. Chem.* 280:29403–29408.
28. Saks, V. A., R. Ventura-Clapier, and M. K. Aliev. 1996. Metabolic control and metabolic capacity: two aspects of creatine kinase functioning in the cells. *Biochim. Biophys. Acta.* 1274:81–88.
29. Saks, V. A., A. V. Kuznetsov, M. Vendelin, K. Guerrero, L. Kay, et al. 2004. Functional coupling as a basic mechanism of feedback regulation of cardiac energy metabolism. *Mol. Cell. Biochem.* 256-257:185–199.
30. Schlattner, U., M. Tokarska-Schlattner, and T. Wallimann. 2006. Mitochondrial creatine kinase in human health and disease. *Biochim. Biophys. Acta.* 1762:164–180.
31. Epand, R. F., M. Tokarska-Schlattner, U. Schlattner, T. Wallimann, and R. M. Epand. 2007. Cardiolipin clusters and membrane domain formation induced by mitochondrial proteins. *J. Mol. Biol.* 365:968–980.
32. Marcillat, O., C. Perraut, T. Granjon, C. Vial, and M. J. Vacheron. 1999. Cloning, *Escherichia coli* expression, and phase-transition chromatography-based purification of recombinant rabbit heart mitochondrial creatine kinase. *Protein Expr. Purif.* 17:163–168.
33. Henon, S., and J. Meunier. 1991. Microscope at the Brewster angle: direct observation of first-order phase transitions in monolayers. *Rev. Sci. Instrum.* 62:936–939.

34. Vollhardt, D. 1996. Morphology and phase behavior of monolayers. *Adv. Colloid Interface Sci.* 64:143–171.

35. Rodriguez Patino, J. M., C. C. Sanchez, and M. R. Rodriguez Nino. 1999. Structural and morphological characteristics of [β]-casein monolayers at the air-water interface. *Food Hydrocolloids.* 13:401–408.

36. Rodriguez Patino, J. M., C. Carrera Sanchez, and M. R. Rodriguez Nino. 1999. Morphological and structural characteristics of monoglyceride monolayers at the air-water interface observed by Brewster angle microscopy. *Langmuir.* 15:2484–2492.

37. Castano, S., and B. Desbat. 2005. Structure and orientation study of fusion peptide FP23 of gp41 from HIV-1 alone or inserted into various lipid membrane models (mono-, bi- and multibi-layers) by FT-IR spectroscopies and Brewster angle microscopy. *Biochim. Biophys. Acta.* 1715:81–95.

38. Castano, S., B. Desbat, A. Delfour, J. M. Dumas, A. da Silva, et al. 2005. Study of structure and orientation of mesentericin Y105, a bacteriocin from Gram-positive *Leuconostoc mesenteroides*, and its Trp-substituted analogues in phospholipid environments. *Biochim. Biophys. Acta.* 1668:87–98.

39. Saccani, J., S. Castano, F. Beaurain, M. Laguerre, and B. Desbat. 2004. Stabilization of phospholipid multilayers at the air-water interface by compression beyond the collapse: a BAM, PM-IRRAS, and molecular dynamics study. *Langmuir.* 20:9190–9197.

40. Saccani, J., S. Castano, B. Desbat, and D. Blaudez. 2003. A phospholipid bilayer supported under a polymerized Langmuir film. *Biophys. J.* 85:3781–3787.

41. Voros, J. 2004. The density and refractive index of adsorbing protein layers. *Biophys. J.* 87:553–561.

42. Lecompte, M. F., G. Bouix, and K. G. Mann. 1994. Electrostatic and hydrophobic interactions are involved in factor Va binding to membranes containing acidic phospholipids. *J. Biol. Chem.* 269:1905–1910.

43. Blaudez, D., J. M. Turlet, J. Dufourcq, D. Bard, T. Buffeteau, et al. 1996. Investigations at the air/water interface using polarization modulation IR spectroscopy. *J. Chem. Soc., Faraday Trans.* 92:525–530.

44. Blaudez, D., T. Buffeteau, J. C. Cornut, B. Desbat, N. Escafre, et al. 1994. Polarization modulation FTIR spectroscopy at the air-water interface. *Thin Solid Films.* 242:146–150.

45. Castano, S., B. Desbat, and J. Dufourcq. 2000. Ideally amphipathic β-sheeted peptides at interfaces: structure, orientation, affinities for lipids and hemolytic activity of (KL)(m)K peptides. *Biochim. Biophys. Acta.* 1463:65–80.

46. Castano, S., B. Desbat, M. Laguerre, and J. Dufourcq. 1999. Structure, orientation and affinity for interfaces and lipids of ideally amphipathic lytic LiKj(i=2j) peptides. *Biochim. Biophys. Acta.* 1416:176–194.

47. Felder, C. E., J. Prilusky, I. Silman, and J. L. Sussman. 2007. A server and database for dipole moments of proteins. *Nucleic Acids Res.* 35(Web Server issue):W512–W521.

48. Lecompte, M. F., J. Clavilier, C. Rolland, X. Collet, A. Negre-Salvayre, et al. 2005. Effect of 4-hydroxynonenal on phosphatidylethanolamine containing condensed monolayer and on its interaction with apolipoprotein A-I. *FEBS Lett.* 579:5074–5078.

49. Mitchell, P., and J. Moyle. 1969. Estimation of membrane potential and pH difference across the cristae membrane of rat liver mitochondria. *Eur. J. Biochem.* 7:471–484.

50. Nicholls, D. G. 1974. The influence of respiration and ATP hydrolysis on the proton-electrochemical gradient across the inner membrane of rat-liver mitochondria as determined by ion distribution. *Eur. J. Biochem.* 50:305–315.

51. Lecompte, M. F., A. C. Bras, N. Dousset, I. Portas, R. Salvayre, et al. 1998. Binding steps of apolipoprotein A-I with phospholipid monolayers: adsorption and penetration. *Biochemistry.* 37:16165–16171.

52. Vernoux, N., T. Granjon, O. Marcillat, F. Besson, and C. Vial. 2006. Interfacial behavior of cytoplasmic and mitochondrial creatine kinase oligomeric states. *Biopolymers.* 81:270–281.

53. Surewicz, W. K., H. H. Mantsch, and D. Chapman. 1993. Determination of protein secondary structure by Fourier transform infrared spectroscopy: a critical assessment. *Biochemistry.* 32:389–394.

54. Marsh, D. 1996. Lateral pressure in membranes. *Biochim. Biophys. Acta.* 1286:183–223.

55. Comte, J., B. Maisterrena, and D. C. Gautheron. 1976. Lipid composition and protein profiles of outer and inner membranes from pig heart mitochondria. Comparison with microsomes. *Biochim. Biophys. Acta.* 419:271–284.

56. Schlame, M., D. Rua, and M. L. Greenberg. 2000. The biosynthesis and functional role of cardiolipin. *Prog. Lipid Res.* 39:257–288.

57. Fritz-Wolf, K., T. Schnyder, T. Wallimann, and W. Kabsch. 1996. Structure of mitochondrial creatine kinase. *Nature.* 381:341–345.

58. Bagatolli, L. A. 2006. To see or not to see: lateral organization of biological membranes and fluorescence microscopy. *Biochim. Biophys. Acta.* 1758:1541–1556.

59. Nelson, A., and F. A. M. Leermakers. 1990. Substrate-induced structural changes in electrode-adsorbed lipid layers. Experimental evidence from the behaviour of phospholipid layers on the mercury-water interface. *J. Electroanal. Chem.* 278:73–83.

60. Golczak, M., A. Kirilenko, J. Bandorowicz-Pikula, B. Desbat, and S. Pikula. 2004. Structure of human annexin a6 at the air-water interface and in a membrane-bound state. *Biophys. J.* 87:1215–1226.

61. Mazon, H., O. Marcillat, E. Forest, and C. Vial. 2005. Local dynamics measured by hydrogen/deuterium exchange and mass spectrometry of creatine kinase digested by two proteases. *Biochemistry.* 87:1101–1110.

62. Saks, V. A., V. V. Kupriyanov, G. V. Elizarova, and W. E. Jacobus. 1980. Studies of energy transport in heart cells. The importance of creatine kinase localization for the coupling of mitochondrial phosphorylcreatine production to oxidative phosphorylation. *J. Biol. Chem.* 255:755–763.

63. Kottke, M., T. Wallimann, and D. Brdiczka. 1994. Dual electron microscopic localization of mitochondrial creatine kinase in brain mitochondria. *Biochem. Med. Metab. Biol.* 51:105–117.

64. Rojo, M., R. Hovius, R. A. Demel, K. Nicolay, and T. Wallimann. 1991. Mitochondrial creatine kinase mediates contact formation between mitochondrial membranes. *J. Biol. Chem.* 266:20290–20295.

65. Beutner, G., A. Ruck, B. Riede, and D. Brdiczka. 1998. Complexes between porin, hexokinase, mitochondrial creatine kinase and adenylate translocator display properties of the permeability transition pore. Implication for regulation of permeability transition by the kinases. *Biochim. Biophys. Acta.* 1368:7–18.

66. Quinn, P. J., and R. M. Dawson. 1969. Interactions of cytochrome *c* and [14C]]-carboxymethylated cytochrome *c* with monolayers of phosphatidylcholine, phosphatidic acid and cardiolipin. *Biochem. J.* 115:65–75.

67. Choi, S. Y., F. Gonzalvez, G. M. Jenkins, C. Slomianny, D. Chretien, et al. 2007. Cardiolipin deficiency releases cytochrome *c* from the inner mitochondrial membrane and accelerates stimuli-elicited apoptosis. *Cell Death Differ.* 14:597–606.

68. Ott, M., V. Gogvadze, S. Orrenius, and B. Zhivotovsky. 2007. Mitochondria, oxidative stress and cell death. *Apoptosis.* 12:913–922.

69. Lutter, M., M. Fang, X. Luo, M. Nishijima, X. Xie, et al. 2000. Cardiolipin provides specificity for targeting of tBid to mitochondria. *Nat. Cell Biol.* 2:754–761.

70. Gonzalvez, F., J. J. Bessoule, F. Rocchiccioli, S. Manon, and P. X. Petit. 2005. Role of cardiolipin on tBid and tBid/Bax synergistic effects on yeast mitochondria. *Cell Death Differ.* 12:659–667.